One-step fabrication of chitosan/dialdehyde cellulose/polypyrrole composite nanofibers with antibacterial, antioxidant, and immunomodulatory effects

One-step fabrication of chitosan/dialdehyde cellulose/polypyrrole composite nanofibers with antibacterial, antioxidant, and immunomodulatory effects

Monika Muchová[a], Lukáš Münster[a], Kristýna Valášková[a], Lenka Lovecká[a], Zdenka Víchová[a], Josef Osička[a], Věra Kašpárková[a,b], Petr Humpolíček[a,b], Ondřej Vašíček[a,c,*], Jan Vícha[a,]**

[a]Centre of Polymer Systems, Tomas Bata University in Zlín, tě. Tomaěe Bati 5678, 760 01 Zlín, Czech Republic

[b]Department of Fat, Surfactant and Cosmetics Technology, Faculty of Technology, Tomas Bata University in Zlín, nam. T. G. Masaryka 5555, 760 01 Zlín, Czech Republic

[c]Institute of Biophysics of the Czech Academy of Sciences, Kmlovopolska 135, 612 00 Brno, Czech Republic

*Correspondence to: O. Vašíček, Institute of Biophysics of the Czech Academy of Sciences, Královopolská 135, 612 00 Brno, Czech Republic.

[**]Correspondence to: J. Vícha, Centre of Polymer Systems, Tomas Bata University in Zlín, tř. Tomáše Bati 5678, 760 01 Zlín, Czech Republic. E-mail addresses: ondrej.vasicek@ibp.cz (O. Vasícek), jvicha@utb.cz (J. Vícha).

ABSTRACT

The study introduces a novel method for fabricating crosslinked chitosan/polypyrrole (PPy) composite nanofibers with covalently anchored PPy. Crosslinking is achieved already during electrospinning by using dialdehyde cellulose (DAC) as a dual-functioning reagent able to simultaneously crosslink chitosan nanofibers and covalently tether PPy nanoparticles by a newly discovered aldol condensation reaction. The presented method eliminates the need for postprocessing steps. It reduces the environmental impact by avoiding toxic organic chemicals while preventing PPy leaching and improving prepared composite nanofibers' mechanical and biological properties. A direct comparison to neat chitosan nanofibres was performed to demonstrate the superiority of prepared composites. The resulting crosslinked $CHIT\_DAC\_PPy$ composite nanofibers have increased tensile strength, improved stability at low pH, conductivity up to 11 mS/cm, and higher swelling compared to neat $CHIT$ nanofibers. They also possess significantly enhanced antibacterial activity against gram-positive S. aureus, higher antioxidant activity, increased immunomodulatory effects, and substantially higher acceleration of wound healing in vitro. $CHIT\_DAC\_PPy$ nanofibrous composite thus shows significant potential for fabricating advanced wound dressings.

Keywords: Nanofibers, chitosan, polypyrrole

1. Introduction

Chitosan, an N-deacetylated derivative of chitin, is a natural biopolymer derived primarily from the exoskeletons of crustaceans such as crabs, shrimp, and lobsters. It comprises β-(1 $\rightarrow$ 4)-linked D-glucos-amine and N-acetyl-D-glucosamine units. Due to its unique properties, including biodegradability, biocompatibility, antimicrobial activity, and mucoadhesivity, chitosan has garnered significant attention in various scientific and industrial fields [**1**]. It is used for various materials, from hydrogels, membranes, and scaffolds to nanofibers [**2**].

Electrospun chitosan nanofibers are particularly interesting due to their fibrous structure, high surface area, and adjustable porosity, which make them excellent candidates for the fabrication of antibacterial wound dressings and for promoting tissue regeneration [**2-4**]. For instance, the morphological analogy of chitosan nanofibers and the extracellular matrix accelerated wound healing processes [**5**]. Chitosan is often electrospun with polyethylene oxide (PEO), improving its spinnability [**6**]. Chitosan nanofibers can also activate macrophages, a prerequisite for initiating and maintaining natural healing processes [**7,8**]. They are also known for their antibacterial properties, being able to disrupt microbial membranes by electrostatic interactions [**9**].

Polypyrrole (PPy) is a conductive polymer highly valued in biomedicine due to its low toxicity and ability to promote cell adhesion, growth, and differentiation [**10-12**]. Conductive PPy materials can promote the growth and proliferation of various cell types, including nerve, chromaffin, and endothelial cells, as well as wound healing and tissue regeneration [**13-15**]. In essence, the formation of the wound changes transepithelial potential within the wounded tissue. If conductive material (PPy) is present, a difference in potentials generates a weak electrical field. This field can promote cell migration and enhance the healing process [**14**]. This phenomenon is known as gal-vanotaxis. Additionally, PPy exhibits antibacterial, antioxidant, antiinflammatory, and immunostimulatory properties [**13**], which may further aid wound healing, regulate cell migration, and stimulate new tissue growth [**16,17**]. Therefore, PPy not only enhances cellular activities but also contributes to a more effective and faster wound-healing process [**18**]. Properties of PPy thus offer a synergy with those of chitosan [**19**]. PPy colloidal nanoparticles are highly interesting for these purposes as they feature a large surface area, have a low polydispersity, allow easy handling, and can be prepared by environmentally friendly synthesis [**20**]. On the other hand, the nanoscale dimensions of PPy colloidal particles pose a considerable challenge in localizing their effects and preventing leaching from composites. For instance, consider a composite made of PPy nanoparticles and chitosan nanofibers. Because PPy is relatively inert, PPy particles are usually only dispersed within the nanofibers [**21**]. When such composite is in contact with water, chitosan nanofibers swell, the distance between polymer chains increases, and untethered PPy particles may no longer be physically entrapped. Leaching of PPy particles degrades composites' properties and may pose health and environmental concerns.

The possible answer is to crosslink chitosan nanofibers and, if possible, covalently anchor PPy within their structure. Currently, however, no strategy for a combined crosslinking of chitosan nanofibers and PPy anchoring has been published, as even the methods for crosslinking chitosan nanofibers are rather complex and require postprocessing steps. For instance, chitosan nanofibers can be crosslinked by exposure to highly toxic glutaraldehyde (GA) vapors, which bring severe health and environmental risks [**22-25**]. Furthermore, materials crosslinked with GA may exhibit considerable cytotoxicity [**26-28**], and highly toxic GA could even be released into the human body during material degradation [**29**].

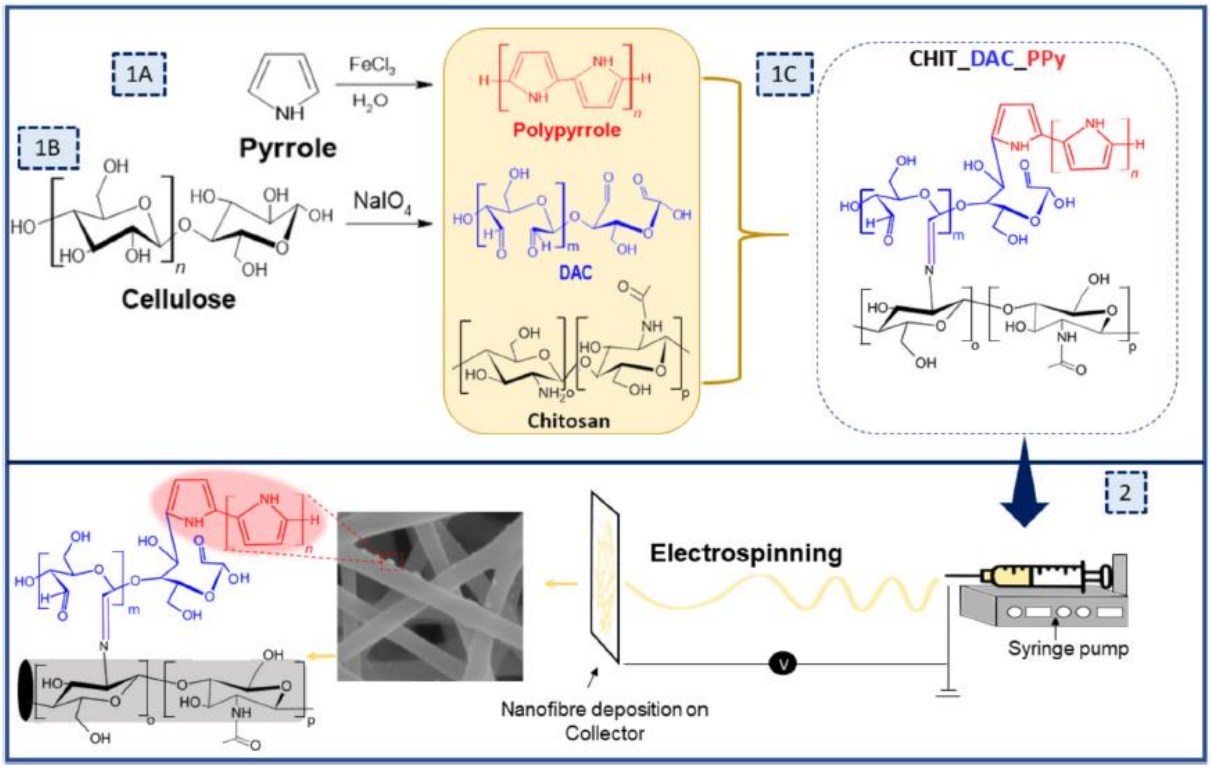

Scheme 1. Overview of experimental effort. 1A) Oxidation of pyrrole to polypyrrole (PPy); 1B) Periodate oxidation of cellulose to 2,3-dialdehyde cellulose (DAC); 1C) Simultaneous Schiff base formation between chitosan and DAC and aldol condensation reaction between polypyrrole and DAC; 2) Electrospinning of $CHIT\_-DAC\_PPy$ solution and production of composite nanofibers.

Here, we report a novel method for the single-step fabrication of conductive composite nanofibrous mats based on crosslinked chitosan and covalently anchored polypyrrole (PPy) nanoparticles. Advantageously, both chitosan crosslinking and PPy anchoring are achieved already during electrospinning by a single reagent - the 2,3-dialdehyde cellulose (DAC). DAC is synthesized by regioselective periodate oxidation of cellulose, resulting in the formation of a pair of aldehyde groups and the cleavage of the $C2-C3$ bond in the anhydroglucose units [**30**]; see **Scheme 1**. DAC has significantly lower toxicity and higher crosslinking effectivity at lower concentrations compared to GA [**27,31-33**], with the added advantage of being derived from renewable sources. While DAC crosslinks chitosan by known Schiff-base chemistry, the colloidal PPy nanoparticles are bound by a recently discovered aldol condensation reaction between terminal pyrrole cycles of PPy and aldehyde groups of DAC, see **Scheme 1** [**19**]. Binding prevents the leaching of PPy particles and further improves the properties of the final composite. To the best of our knowledge, the DAC has not yet been used as a crosslinker for chitosan nanofibers despite its known applications in preparing chitosan hydrogels [**26,34**]. This is most likely because crosslinking of chitosan nanofibers typically requires immersion in a DAC solution, which could cause swelling of nanofibers accompanied by (partial) loss of structure and other undesirable effects.

The novelty of the presented approach thus lies in the use of DAC as a dual-functioning agent for the fabrication of conductive composite nanofiber chitosan/PPy mats already during the electrospinning process, which is i) simplifying the production of crosslinked chitosan nanofibers by eliminating the need for further postprocessing, ii) enhancing environmental safety by avoiding toxic organic chemicals iii) increasing composite durability by preventing PPy leaching and iv) improving the mechanical, chemical and biological properties of the final composite. A direct comparison to neat

chitosan nanofibres was performed to demonstrate the advantages of prepared composites, particularly in biomedical applications.

Thus, the working hypothesis is that the DAC could prepare conductive crosslinked chitosan/polypyrrole composite nanofibers with enhanced properties directly during electrospinning without needing postprocessing steps or toxic organic chemicals.

2. Material and methods

2.1. Materials

Medium molecular weight chitosan (448877, Sigma Aldrich Co.), degree of deacetylation 76 % (for NMR spectrum, see Fig. S3), $M_w = 288$ kDa, dispersity $Đ = 6.7$, Cellulose SigmaCell type 20 with M_w = 76 kDa, $Đ = 4.7$ (S3504, Sigma Aldrich Co.), polyethylene oxide (PEO; M_v = 600 kDa, Sigma Aldrich Co.), poly(vinylpyrrolidone) (PVP, $M_w = 360$ kDa), Fluka. Sodium periodate ($NaIO_4$), Penta, Czech Republic, ethylene glycol, Penta, Czech Republic, pyrrole, Sigma-Aldrich, iron (III) chloride ($FeCl_3$), Sigma-Aldrich. The materials for biological evaluation are provided in the SI (see section S1.2). All chemicals were of analytical grade and were employed without additional purification.

2.2. Preparation of DAC, PPy, and $CHIT\_DAC\_PPy$ chitosan nanofibers

To obtain DAC, the cellulose was oxidized using a 1.2× molar excess of $NaIO_4$ at 30 ° C for 72 h, as described in previous works [**27,32,35**]. The reaction was stopped by the addition of ethylene glycol, and the resulting product was purified via several cycles of centrifugation (9000 RPM for 15 min using a Thermo Fisher Scientific Sorvall LYNX 4000 centrifuge) and homogenization (1000 RPM for 10 min with a Witeg WiseTis HG-15D homogenizer). Subsequently, the suspension was solubilized at 80 °C under reflux for 2 h. After removing impurities through centrifugation and filtration, the resulting solution was dialyzed for 24 h using a 14 kDa molecular weight cut-off ($MWCO$) membrane and then lyophilized. The degree of oxidation of the resulting soluble DAC was determined by oxime reaction and alkalimetric titration to be 94 $\pm$ 2 % based on a previously published methodology [**27**]. Briefly, 100 mg of DAC was dissolved in 30 mL of water, and the pH was set to 4. The solution of 430 mg of hydroxylamine hydrochloride in 20 mL of water (pH 4) was added to a solution of DAC and stirred for 24 h at laboratory temperature. The conversion of aldehydes to oxime was determined based on consumption of 0.1 N NaOH.

To determine molecular weight, DAC was converted to 2,3-dicarbox-ycellulose by chlorite following our earlier works [**35,36**]. This method allows a more reliable determination of the molecular weight of rather reactive DAC and was shown to be particularly relevant for hydrogel crosslinkers, whose molecular weights determined by this method well correlated with the properties of final hydrogels [**27**]. Briefly, to prepare 2,3-dicarboxycellulose, 100 mg of DAC was oxidized for 24 h using 4 times molar excess of $NaClO_2$ (0.1 M, in 0.5 M acetic acid). The reaction was terminated by NaOH (pH set to 8.5) and the product was purified by dialysis, filtered, and lyophilized. The Mw of resulting 2,3-dicarboxycel-lulose was 14 kDa ($Đ = 1.65$), which corresponds to $DP = 60$ and M_w of DAC 10 kDa. Relatively low M_w value is caused by the solubilization process required to obtain water-soluble DAC.

To synthesize PPy colloid, 25 mL of 2 wt% PVP solution in ultrapure water (UPW) was prepared, and 0.335 g of pyrrole (5 mmol) in 25 mL UPW was added. The mixture was then sonicated for 30 min. Following sonication, 50 mL of an oxidizing agent solution containing 1.352 g of FeCL was added. After

24 h of reaction, dialysis was carried out against a 0.2 M HCl solution using a 7 kDa $MWCO$ membrane [**13**]. Based on gravimetric analysis, 1 mL of the final colloid contained 21.9 mg of particles.

Chitosan/dialdehyde/polypyrrole nanofibrous composite ($CHIT\_-DAC\_PPy$) was prepared as follows: Chitosan was dissolved in 87.5 % acetic acid at a concentration of 25 mg/mL. The amount of PPy colloid containing 5 wt% or 10 wt% of PPy particles relative to chitosan was added to the filtered chitosan solution. Subsequently, DAC (3 mol% relative to $CHIT$) and PEO ($CHIT$: PEO 4:1 w/w) were dissolved in water and added to the solution of $CHIT$ and PPy. Adding polyethylene oxide (PEO) as a co-spinning agent improves the spinnability of chitosan and enhances fiber morphology [**6,37**]. The final solution contained chitosan in the concentration of 20 mg/mL, in 70 % acetic acid, 3 mol% DAC relative to $CHIT$, PEO (20 wt% relative to $CHIT$), and PPy (5 wt% or 10 wt% relative to $CHIT$). $CHIT\_DAC$ was fabricated similarly only without PPy, and CHIT was prepared without both DAC and PPy and using the ratio $CHIT$: PEO 5:1. The $CHIT\_DAC\_PPy$ mixture had a dynamic viscosity of 2.75 Pa.s and conductivity of 805 μS/cm, and other were similar. All mixtures were subsequently degassed and fed into the 16 nozzles of the SpinLine 40 device (SPUR a.s., Czech Republic) at the following rates: $CHIT$ = 0.53 mL/min, $CHIT\_DAC$ = 0.43 mL/min, $CHIT\_DAC\_PPy$ 5 % in the range of 0.39 mL/min, and $CHIT\_DAC\_PPy$ 10 % in the range of 0.48 mL/min. A spinning voltage of 60 kV was applied with a working distance of 20 cm while maintaining a relative humidity of 25-28 %. Chitosan nanofibers were electrostatically spun onto a polypropylene (PP) substrate, each cycle lasting 60 min.

2.3. Physico-chemical characterization

Infrared spectroscopy ($FT-IR$). A qualitative spectral analysis of the prepared DAC, PPy, $CHIT$, $CHIT\_DAC$, and $CHIT\_DAC\_PPy$ was conducted using an $FT-IR$ spectrometer (Nicolet 6700, Thermo Fisher Scientific, USA) with a diamond crystal and ATR mode. The wavenumber range covered by the spectral analysis was 4000 to 400 cm^{-1}.

Ultraviolet-visible spectroscopy ($UV-Vis$). A Lambda 1050 two-beam UV-Vis spectrometer (PerkinElmer, USA) was used to measure the absorbance of the PPy solution in the 200-800 nm wavelength range.

Transmission electron microscopy (TEM) analysis. A JEM-2100 transmission microscope (JEOL, Japan, accelerating voltage 160 keV) was used. Samples were deposited on a Formvar membrane-coated 300 mesh copper grid.

Dynamic light scattering (DLS) analysis. Measurements of zeta potential (ξ) and hydrodynamic radii were performed using Zetasizer Nano ZS90 Malvern Instruments, UK) at 25 °C.

Network parameters of crosslinked nanofibers. The network parameters were determined based on swelling of 3 × 3 cm specimens of $CHIT$, $CHIT\_DAC$, $CHIT\_DAC\_PPy$ 5 %, and $CHIT\_DAC\_PPy$ 10 % nanofiber samples in UPW. The swollen samples were gently dried, weighed, and lyophilized. The equilibrium swelling theory of Flory and Rehner was used to calculate the network parameters [**38**]. Formulas for calculating network parameters are shown in the SI (see Section S1.1).

SEM analysis. A Nova NanoSEM 450 (FEI, Czech Republic, 5 kV accelerating voltage) was used. Samples were sputtered by gold-palladium nanoparticles to prevent the charge accumulation effect.

Mechanical properties. The tensile tests were measured using a Tes-tometric M350-CT device, with a speed of 50 mm/min and a sample length of 30 mm.

Conductivity measurements. A van der Pauw four-electrode method (digital electrometer Keithley 6517B; voltage source Keithley 2410; scanner Keithley 7002) was used. Measurements were conducted at 25 °C.

NMR spectroscopy: The 1H NMR spectra of 10 mg/mL chitosan solution were measured using a JEOL 400 MHz NMR spectrometer (JEOL, Japan) at $T = 298$ K in D_2O/DCl (0.1 M) mixture with presaturation. The degree of deacetylation was determined based on Kasaai et al. [**39**].

Gel permeation chromatography: Reported molecular weights are apparent values obtained by analysis on a Waters HPLC Breeze chromatographic system (Waters, USA) equipped with a refractive index detector Waters 2414 (drift tube $T = 60$ °C) and a Tosoh TSK gel GMPWXL column (300 mm × 7.8 mm × 13 μm, column $T = 30$ °C). The mobile phase for 2,3-dicarboxycellulose consisted of a mixture of 0.1 M $NaNO_3$ and 0.05 M Na_2HPO_4-$12H_2O$. The mobile phase for chitosan consisted of 0.2 M ammonium acetate buffer. Flow rate of 0.8 mL/min was used. Pullulan polysaccharide calibration kit SAC-10 (M_w = 342-805,000 g/mol, Agilent Technologies, USA) was used in all cases.

2.4. Biological evaluation

Cytocompatibůity. Cytocompatibility assessments involved examining the cytotoxicity of chitosan nanofibers and observing cell growth in direct contact with the material. Cytotoxicity of chitosan nanofibers was tested on NIH/3T3 cells (ECACC 93061524, England) using the MTT assay (ISO 10993-5). Cells were incubated with nanofibers for 24 h at 37 °C in 5 % CO_2. Viability was measured at 570 nm using the Infinite M200 Pro NanoQuant (Tecan, Switzerland). According to ISO 10993-5, viability above 0.7 indicates non-cytotoxicity, while values below 0.7 are considered cytotoxic.

For cell growth, cells were seeded, incubated for 48 h, fixed, and stained with Hoechst 33258 and ActinGreen™ 488. Cell morphology was observed with an Olympus Fluoview FV3000 confocal microscope (Olympus, Japan). Further details are provided in the SI (see S1.2 Biological Evaluation).

Oxidative burst in isolated neutrophils. Blood samples were collected from healthy adults (18-50 years old, both genders) without recent treatments or illness and preserved using sodium citrate (0.38 %) as an anticoagulant. Immune cells from healthy donors were isolated from buffy coats. These were obtained from the Department of Transfusion and Tissue Medicine of the Brno University Hospital, under a contract approved by the ethical committee of FH Brno. Neutrophil viability was confirmed (>95 %) using CellDrop (DeNovix, USA). ROS formation by isolated neutrophils was monitored by luminol-enhanced chemiluminescence over 120 min at 37 °C (Tecan Infinite M200), according to [**40**]. Additional details can be found in the SI (see S1.2 Biological Evaluation).

Antioxidant activity. The antioxidant activity of electrospun nanofibers was evaluated using a cell-free luminol-HRP-H_2O_2 system, using hydrogen peroxide (H_2O_2) and horseradish peroxidase (HRP) [**41**]. In this assay, chemiluminescence (CL) was initiated in a medium containing electrospun nanofibers, H_2O_2 (100 μmol/L), HRP (2 U/mL), and luminol (10 μM). The CL signal was recorded for 120 min at 37 °C using a luminometer (Infinite M200, Tecan, Switzerland). Results were normalized to the control and reported as mean ($n = 4$) $\pm$ standard error. Further details are provided in the SI (see S1.2 Biological Evaluation).

IL-6 and NO production of murine macrophages and their viability. The cytotoxicity of nanofibers was tested on RAW 264.7 cells using an MTT assay [**42,43**]. Cells were incubated with the nanofibers and lipopoly-saccharides (LPS, 15 ng/mL, $E.coli$/026:B6, Sigma-Aldrich Co.) for 24 h at 37 °C in an atmosphere containing 5 % CO_2 and 95 % air. After incubation, cell viability was determined using the

MTT assay and measured with a SPECTRA Sunrise microplate reader (Tecan, Man-nedorf, Switzerland). NO levels were measured using Griess reagent, and IL-6 levels were measured using Mouse IL-6 DuoSet (R&D Systems) [**44**]. Data were normalized to the control (with LPS) and presented as mean ($n = 4$) ± standard error of the mean. Further details are provided in the SI (see S1.2 Biological Evaluation).

In vitro wound healing. The scratch assay was performed to evaluate the wound-healing potential of nanofibers using NIH/3T3 mouse embryonic fibroblast cell line, as described by [**45**]. Cells were seeded onto tissue culture plates at a density of 2 × 105 cells per mL and incubated at 37 °C with 5 % CO_2 in a humidified atmosphere until they formed a confluent monolayer. A scratch was then introduced using a sterile pipette tip, followed by rinsing the remaining cells with PBS to remove any debris, and images of the initial scratch were recorded. Fresh medium containing the test samples was then added, and plates were incubated under the same conditions. Cell migration was monitored, and images were captured at 0 h and 10 h using an Olympus IX81 phase-contrast microscope (Olympus, Japan). Wound closure was quantified using T-Scratch software (CSElab, Switzerland), with results presented as the percentage of open wound area remaining at 0 and 10 h.

Antibacterial activity. The antibacterial properties of nanofibrous mats were tested following ISO 20743 and ISO 22196 standards, which describe the antimicrobial efficacy properties and test methods for plastic products, filters, nanofibres, or light and porous samples. Testing according to these standards assesses the ability of samples to inhibit (bacteriostatic properties) or kill (bactericidal properties) microorganisms over 24 h. In our study, we used a slightly modified methodology to accommodate the specific characteristics of our samples, namely their light and porous nature, which do not meet weight parameters for the standard test. A detailed description of the procedure follows: Antibacterial performance was assessed using gram-positive bacteria Staphylococcus aureus CCM 4516 and gram-negative bacteria Escherichia coli CCM 4517 (sourced from CCM, Brno, Czech Republic). These bacterial strains were cultivated on plate count agar (PCA). For the nanofibrous mats, a process was undertaken wherein sterile samples measuring 2 × 2 cm were inoculated with a volume of 0.1 mL of a bacterial suspension containing a known number of microorganisms diluted in 1/500 nutrient broth (NB). Following this initial inoculation, the samples were incubated for 24 h at 35 °C and relative humidity ≥90 %. Once the incubation period concluded, the samples were neutralized and rinsed with a specialized SCDLP solution (the Soybean Casein Digest Lecithin Polysorbate Medium). Obtained bacterial extracts were serially diluted, and to assess the viability of the bacteria present, colony counts were systematically conducted on PCA agar plates, allowing for a comprehensive evaluation of the bacterial population. All tests were performed in duplicates, and structurally similar PUR nanofiber mats without known antibacterial activity were used as reference material.

The antimicrobial activity (A) is calculated using the formula:

$$A = logS_{xh} - logS_{0h} \quad (1)$$

where A is antibacterial activity; $logS_{xh}$ is the common logarithm of the arithmetic average of the number of bacteria obtained from functionalized samples after 24 h of incubation; and $logS_{0h}$ is the common logarithm of the arithmetic average of the number of bacteria obtained from functionalized samples after 0 h of incubation.

The effectiveness of the antibacterial activity was evaluated according to EN ISO 20743:2021 - Textiles - Determination of the antibacterial activity of textile products, and the effectiveness values are given in Table S3.

2.5. Statistical analysis

Statistical analysis was performed using GraphPad Prism version 6.01. Statistical differences were tested by one-way ANOVA, followed by Dunnett's multiple comparison test or by a one-sample t-test to compare values expressed as percentages. In the case of one sample t-test application, the Bonferroni correction of the p-value for multiple comparisons was performed. $P < 0.05$ was taken to indicate significant differences between data mean values.

3. Results and discussion

3.1. Chemical characteristics of the nanofibers and composites

Initially, DAC was prepared following earlier works [**27,32,35**], lyophilized and characterized by $FT-IR$ spectroscopy (**Fig. 1**). The infrared spectrum of DAC exhibits a characteristic absorption band of $C=O$ at 1730 cm^{-1}, confirming the successful oxidation of cellulose, and the increase in intensity of the $C-O-C$ vibration band at 885 cm^{-1}, caused by the formation of various hemiacetals in DAC [**46**].

Next, the PPy colloid stabilized with PVP was prepared (particle concentration of 21.9 mg/mL) and characterized using $FT-IR$, UV-Vis spectroscopy, DLS, and TEM analysis. The $FT-IR$ spectrum (PPy, **Fig. 1**) displayed characteristic vibrational bands of PPy, including $C-C$ stretching vibrations between 1440 and 1560 cm^{-1} and $C—H$ wagging vibrations in the range of 800-1000 cm^{-1}, confirming PPy's molecular structure.

In the $UV-Vis$ spectrum (**Fig. 2**A), an absorption peak around 400 nm indicates the $\pi-n^{*}$ transition due to polarons. An increase in absorbance from 600 to 800 nm represents the localized polaron band associated with the conductive properties of oxidized PPy [**47**]. The hydrodynamic diameter of the particles according to DLS was 188 ± 4 nm (see **Fig. 2**B), and the polydispersity index (PDI) was 0.23, indicating a relatively narrow particle size distribution. TEM analysis revealed spherical PPy nanoparticles of 35 ± 3 nm in diameter (**Fig. 2**C). Colloidal solutions also remained stable for a year in PBS with pH 7.4 without showing any signs of coalescence or agglomeration [**13**].

Subsequently, $CHIT$ nanofibers, $CHIT$ nanofibers crosslinked by DAC ($CHIT\_DAC$), and composite formed by $CHIT$ nanofibers crosslinked by DAC with 5 or 10 wt% of PPy colloidal particles ($CHIT\_DAC\_PPy$ 5 % or $CHIT\_DAC\_PPy$ 10 %) were electrospun, see **Section 2.2** for more details. The $FT-IR$ spectrum of neat $CHIT$ nanofibers (**Fig. 1**) exhibits characteristic absorption bands of chitosan at 1650 cm^{-1} (vibration of amide I from N-acetyl groups), 1565 cm^{-1} (bending vibration of $N—H$ from primary amine), and stretching vibration of $C—O$ at 1075 and 1030 cm^{-1} [**48**]. The Schiff base formation between the -NH_2 group of chitosan and the -CHO group of DAC in $CHIT\_DAC$ nanofibers is evidenced by the disappearance of $C=O$ vibration of DAC at 1730 cm^{-1} and decrease of the primary amine $N—H$ vibration intensity at 1565 cm^{-1}, and the appearance of an imine bond vibration at 1590 cm^{-1} [**49,50**].

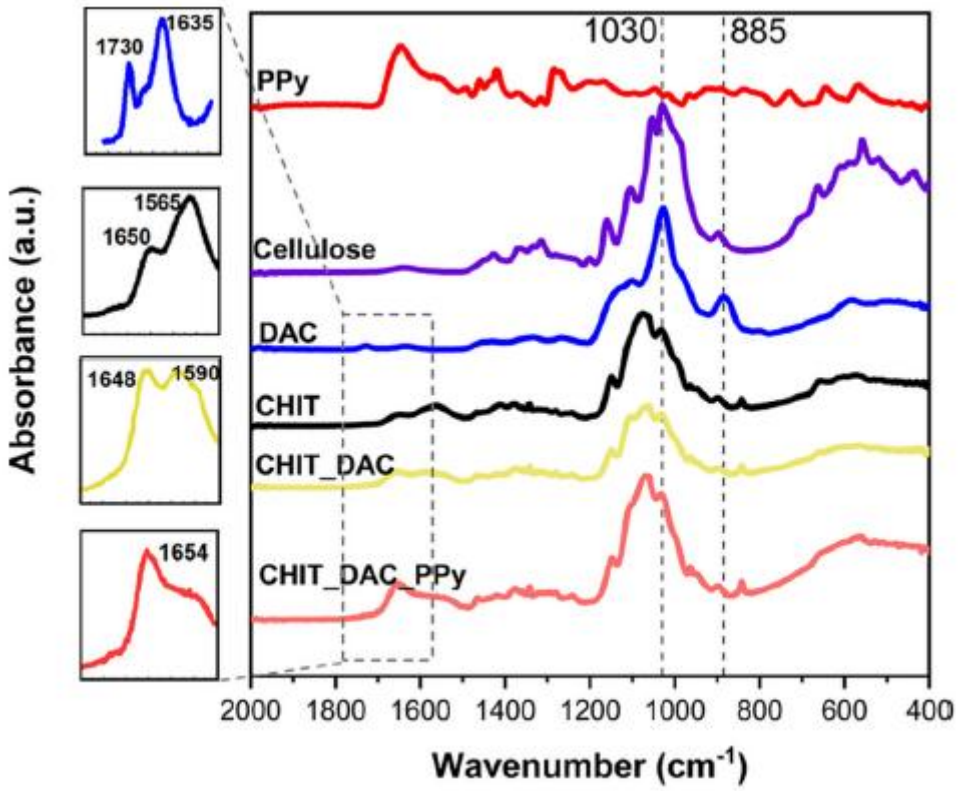

Fig. 1. $FT-IR$ spectra of PPy, cellulose, DAC, and $CHIT$, $CHIT\_DAC$, and $CHIT\_DAC\_PPy$ nanofibers. See Fig. S4 in Supporting information (SI) for full $FT-IR$ spectra.

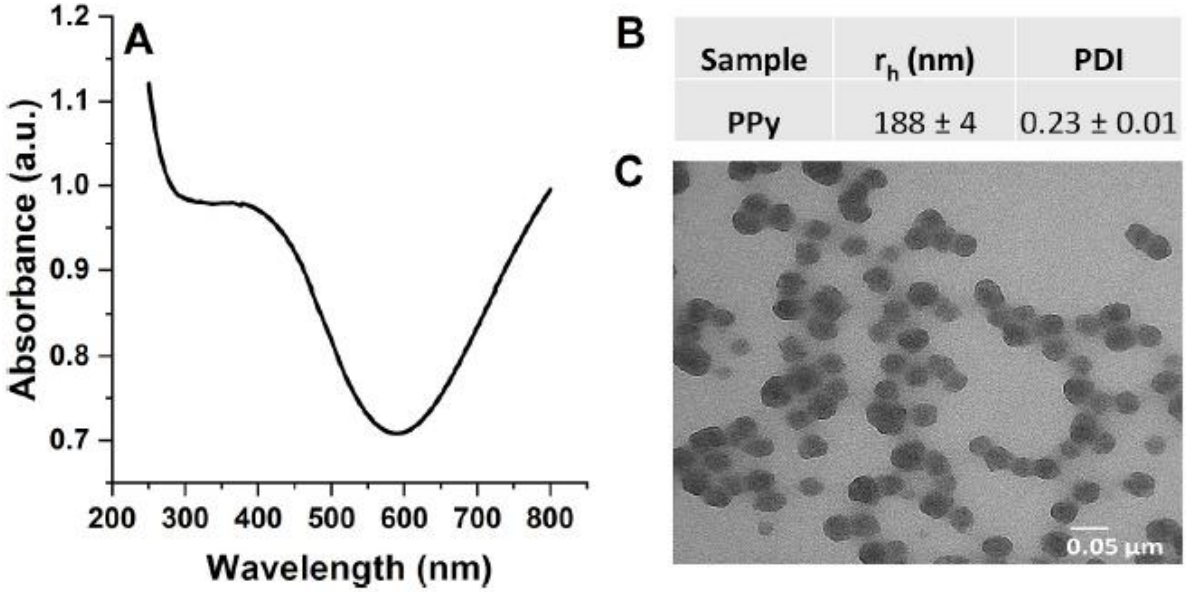

Fig. 2. A) $UV-Vis$ spectroscopy of prepared colloidal PPy and B) their particle size using DLS and C) TEM of PPy colloidal particles.

The aldol condensation between PPy and DAC in the $CHIT\_DAC\_PPy$ nanofiber sample is evidenced by the increased intensity of vibration at 1654 cm^{-1}, which was shown to be a result of DAC and PPy

reaction [**19**]. Other PPy vibrations are also observable in the nanofibrous composite $FT-IR$ spectrum. The evidence of a Schiff base formation between the NH_2 group of chitosan and the -CHO group of DAC in $CHIT\_DAC$ nanofibers is the decrease of the primary amine $N—H$ vibration intensity at 1565 cm^{-1} and the appearance of an imine bond vibration at 1590 cm^{-1} [**49,50**]. The aldol condensation between PPy and DAC in the $CHIT\_DAC\_PPy$ nanofiber sample is evidenced by the increased vibration intensity at 1654 cm^{-1}, which is specific for the formation of $DAC-PPy$ bond [**19**]. Other PPy vibrations are also observable in the $FT-IR$ spectrum of $CHIT\_DAC\_PPy$, proving the presence of PPy particles.

3.2. Physical and morphological characteristics of the nanofibers

Initially, the mechanical properties of the prepared $CHIT$, $CHIT\_DAC$, and composite $CHIT\_DAC\_PPy$ 5 % and $CHIT\_DAC\_PPy$ 10 % nanofibers were characterized in a dry state. Stress-strain curves of individual samples are shown in **Fig. 3**, and measured values are given in **Table 1**.

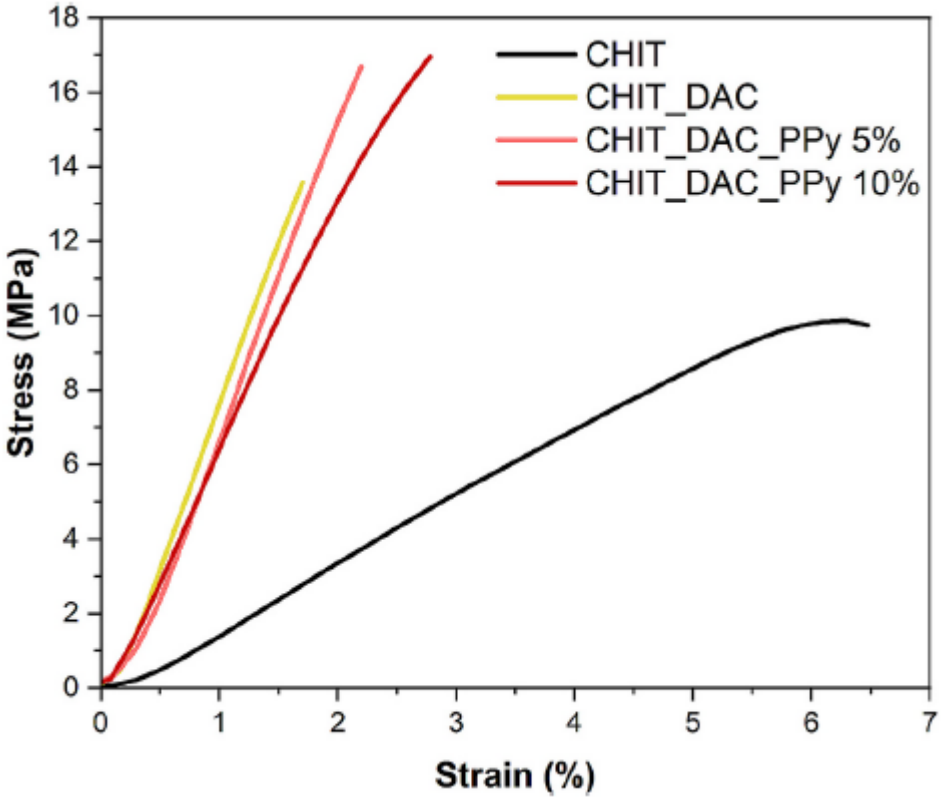

Fig. 3. Examples of stress-strain curves of $CHIT$, $CHIT\_DAC$, $CHIT\_DAC\_PPy$ 5 % and $CHIT\_DAC\_PPy$ 10 % nanofibers.

It was found that neat $CHIT$ nanofibers exhibited lower tensile strength and higher strain than crosslinked ones. This finding is consistent with the fact that chitosan macromolecules in $CHIT$ fibers are predominantly held together by hydrogen bonding and physical entanglement, which allows for certain flexibility between macromolecules and, thus, higher elongation upon stress, resulting in higher measured strain. However, it also translates into lower tensile strength due to the absence of covalent bonds between chitosan chains.

Crosslinking of the fibers with DAC thus leads to an increase in tensile strength and a decrease in strain at break compared to $CHIT$. This phenomenon can be attributed to the strong covalent bonds between $CHIT$ and DAC. Note that both PPy composites feature further decreased strain at break compared to $CHIT\_DAC$, as the presence of stiff and covalently anchored PPy particles results in the higher overall stiffness of the fibers [**21**].

Based on the results obtained and the spectroscopic evaluation performed in the previous section, the crosslinked electrospun $CHIT\_DAC$ nanofibers and their PPy composites could be described as nanofibrous xerogels. Hence, when exposed to the aqueous environment, these xerogels should swell into hydrogels. Subsequent tests thus involved the characterization of swelling, gel fraction, and equilibrium water content of all electrospun nanofiber mats (**Fig. 4**A), followed by SEM analysis of dry/swelled nanofiber diameters (**Fig. 4**B). Photographs of all prepared samples are in **Fig. 4**C.

The swelling of $CHIT$ and $CHIT\_DAC$ was the same within experimental error (700 $\pm$ 120 % for $CHIT$ and 620 $\pm$ 90 % for $CHIT\_DAC$). The relatively low swelling of uncrosslinked $CHIT$ nanofibers is given by a dense hydrogen bond network, which also prevents $CHIT$ dissolution at neutral pH. While crosslinking by DAC replaces part of the hydrogen network by Schiff bases, swelling remains comparable as both effects largely cancel each other. In comparison, both PPy-containing samples swelled significantly more, namely by 950 $\pm$ 80 % for $CHIT\_DAC\_PPy$ 5 % and 1200 $\pm$ 200 % for the $CHIT\_DAC\_PPy$ 10 % sample. The $CHIT\_ - DAC\_PPy$ 10 % sample is thus able to contain nearly two times higher amount of water than $CHIT\_DAC$. Higher swelling is potentially advantageous, as absorbing exudate and maintaining a moist environment are crucial for perspective wound dressings.

Two factors cause the increased swelling of $CHIT\_DAC\_PPy$ samples. First, the presence of PPy nanoparticles embedded in the network disrupts the orderly structure of the chitosan matrix and prevents the formation of hydrogen bridges between chitosan chains. Second, the aldol condensation reaction between DAC and PPy, which is competitive towards imine bond formation, localizes the part of the DAC molecules to the surface of PPy particles. This decreases the number of free DAC molecules available for crosslinking of bulk chitosan matrix and leads to the formation of so-called two-phase network topology [**33**], in which are regions of high crosslink density (PPy particles with bound DAC) embedded in a more sparsely crosslinked matrix. This phenomenon is discussed more in our previous work examining the DAC as a crosslinker for hydrogels [**33**].

EWC (equilibrium water content) largely follows the swelling trend, ranging from 85.9 $\pm$ 1.8 % for $CHIT\_DAC$ fibers to 92.1 $\pm$ 1.2 % for $CHIT\_DAC\_PPy$ 10 %. The gel fraction of the samples ranges from 66.5 $\pm$ 4.5 % for $CHIT\_DAC\_PPy$ 10 % to 84.9 $\pm$ 1.7 % for $CHIT$. Note that gel fraction is influenced by the washing of PEO from the nanofibers.

Table 1 Results of the tensile tests.

Samples	Tensile strength (MPa)	Strain at break (%)	Young's modulus (MPa)	Strain at maximum strength (%)
CHIT	8.6 $\pm$ 2.7	9.3 $\pm$ 2.2	180 $\pm$ 50	8.3 $\pm$ 2.2
CHIT_DAC	14.6 $\pm$ 4.6	5.1 $\pm$ 0.6	690 $\pm$ 180	2.2 $\pm$ 0.3
CHIT_DAC_PPy 5 %	15.9 $\pm$ 3.3	3.3 $\pm$ 0.4	862 $\pm$ 130	1.7 $\pm$ 0.7
CHIT_DAC_Ppy 10 %	17.2 $\pm$ 2.0	3.6 $\pm$ 0.4	770 $\pm$ 90	2.9 $\pm$ 0.2

SEM analysis shows the changes in the structure of the nanofibers before and after swelling; see **Fig. 4**B and Fig. S5 in Supporting information (SI). Nanofiber diameters of the samples before and after washing are as follows: $CHIT$ 73 $\pm$ 20 nm (dry) and 137 $\pm$ 38 nm (swelled), $CHIT\_DAC$ 73 $\pm$ 21 nm (dry) and 124 $\pm$ 41 nm (swelled), $CHIT\_DAC\_PPy$ 5 % 54 $\pm$ 12 nm (dry) and 217 $\pm$ 83 nm (swelled), and $CHIT\_DAC\_PPy$ 10 % 102 $\pm$ 29 nm (dry) and 288 $\pm$ 66 nm (swelled). The most significant increase in nanofiber diameter was thus observed for $CHIT\_DAC\_PPy$ 10 %, consistent with its highest observed swelling.

Fig. 4C further illustrates the macroscopic (up) and microscopic (down) appearances of the prepared nanofibers to better compare structural and morphological changes across samples.

Another advantage of in situ chitosan crosslinking is nanofibers' improved chemical stability. All samples were immersed in HCl solutions of pH = 3 for 24 h under constant shaking. After this period, the samples were gently rinsed and lyophilized. SEM analysis was conducted, see **Fig. 5**. While the $CHIT$ sample completely dissolved during this period and is thus not shown, $CHIT\_DAC$ and $CHIT\_DAC\_PPy$ samples remained undissolved. Their surface also bears evident traces of original nanofibrous structure, see **Fig. 5**. Moreover, PPy particles are still visible as bright dots on the surface of the $CHIT\_DAC\_PPy$ 5 % and $CHIT\_DAC\_PPy$ 10 % samples (**Fig. 5**). PPy particles are thus not washed from the surface of the nanofibers due to DAC-mediated covalent tethering, which presents another advantage of presented fabrication method.

Given the presence of PPy particles, the conductivity of the samples was investigated next. Note, that the conductivity of composites is realized by a combination of ionic/electronic mechanisms due to limited contact between conductive particles below the percolation threshold. Only when the percolation threshold of the dielectric matrix is overcome by increasing the number of conductive particles can a significant increase in conductivity be expected [**21**]. This is, however, not the case, as the conductivity of dried samples was in the order of nS/cm. Contrarily, the conductivity of the samples in the swelled state, which is more relevant given the intended biomedical applications, was significantly higher, being 2.6 $\pm$ 0.2 mS/cm for $CHIT\_DAC\_PPy$ 5 % and 11.6 $\pm$ 0.2 mS/cm for $CHIT\_DAC\_PPy$ 10 %. This is comparable to human muscles (4.1 mS/cm) and dermis (2.2 mS/cm) [**51**]. Also, conductivity increased over four times for twice the amount of PPy, probably due to the approaching percolation threshold. Further increase in the amount of PPy thus may be beneficial if a high increase in conductivity is required.

3.3. Biological evaluation

Initially, cytotoxicity assessment was conducted according to ISO 10993-5 using the mouse embryonic fibroblast $NIH/3T3$ cell line. As shown in **Fig. 6**A, none of the prepared nanofibrous materials exhibited cytotoxicity. Even those containing colloidal polypyrrole, i.e., the $CHIT\_DAC\_PPy$ 5 % and $CHIT\_DAC\_PPy$ 10 %, did not impact cell viability significantly compared to the reference.

Samples were subsequently incubated with $NIH/3T3$ cells for 48 h, and cell growth in their presence was evaluated using confocal microscopy. Tested samples have no impact on the morphology of the fibroblasts (see **Fig. 6**B), which proliferate in their presence. Moreover, cells did not adhere to the surface of samples, which is important for the wound dressings that need to be changed regularly. The cell adhesion properties are most likely limited because PPy does not form a solid film on the nanofiber's surface, and individual particles do not offer sufficient area to support the attachment of cells.

3.3.1. Antioxidant aktivity

Because both chitosan and PPy have antioxidative properties [**52-54**], the scavenging of reactive oxygen species (ROS) was evaluated next.

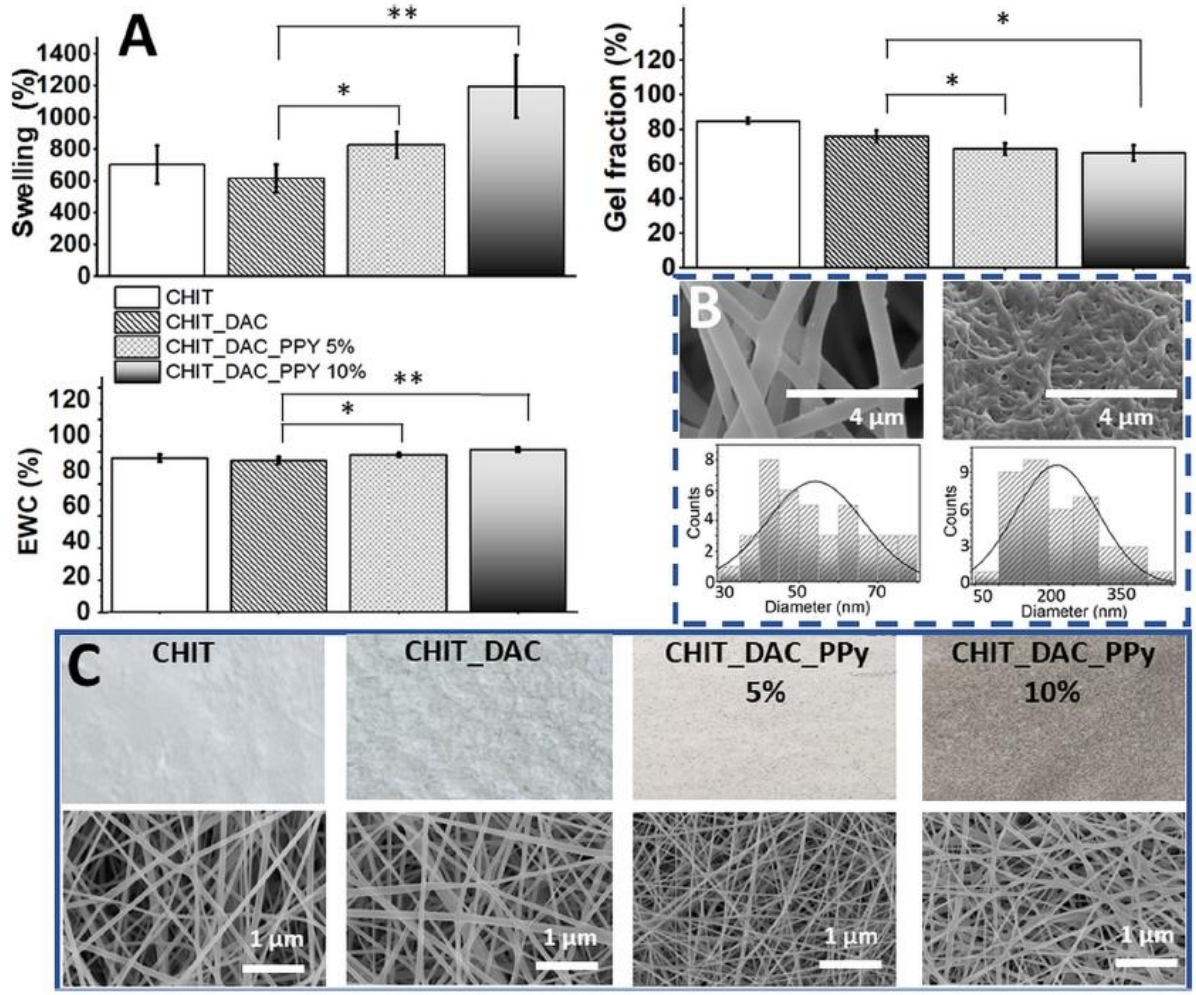

Fig. 4. A) Network parameters of prepared nanofibers, their swelling capacity, gel fraction, and EWC; B) representative SEM images before (left) and after swelling (right) of $CHIT\_DAC\_PPy$ 5 % and respective nanofiber diameter distribution; C) photographs of individual samples and their SEM images. (* $p < 0.05$, ** $p < 0.01$).

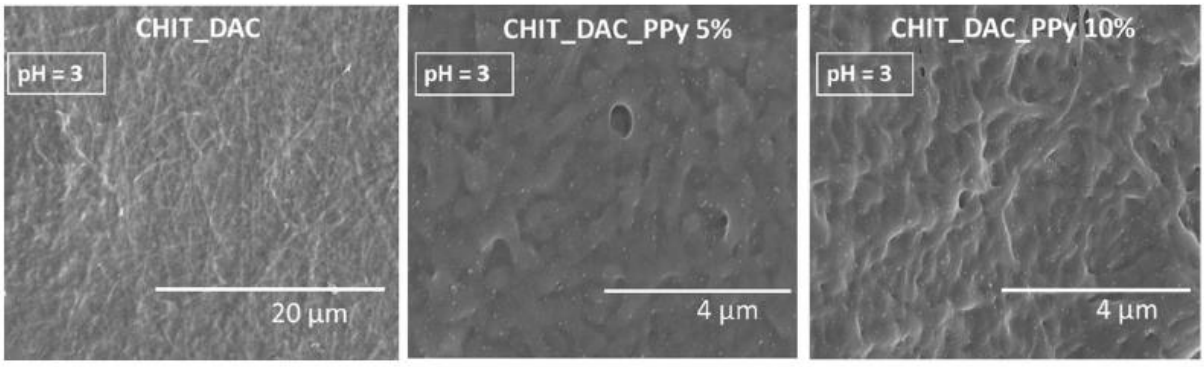

Fig. 5. SEM images of prepared nanofibrous samples in an acidic environment (pH = 3).

The antioxidant activity is crucial during wound healing, as ROS are generated during the inflammatory phase, causing biological damage, including lipid, protein, and nucleic acid degradation. This ultimately leads to cell death and complicates wound healing [**52**]. Initially, we focused on monitoring the antioxidant activity of samples using a luminol-horseradish peroxidase-H_2O_2 cell-free system.

The antioxidant activity results revealed relatively mild antioxidant activity of $CHIT$ and $CHIT\_DAC$, which reduced the response to approximately 74 and 82 % of the positive control, respectively (**Fig. 7**). On the other hand, nanofibers containing PPy showed a much more pronounced effect. The $CHIT\_DAC\_PPy$ 5 % sample decreased the signal to <50 % of the control, while $CHIT\_DAC\_PPy$ 10 % decreased the signal to 27 % of the control. In other words, adding PPy provided a synergic effect with chitosan and showed significantly better antioxidant activity scaling with the amount of PPy compared to $CHIT$ nanofibers.

After confirming the antioxidant activity of the prepared $CHIT$ in a cell-free system, we analyzed their impact on the ROS produced by neutrophils, spontaneously or upon activation by OZP and PMA. The oxidative burst of neutrophils is primarily linked to the production of superoxide anion radicals, the first ROS generated by neutrophils upon interacting with various exogenous stimuli.

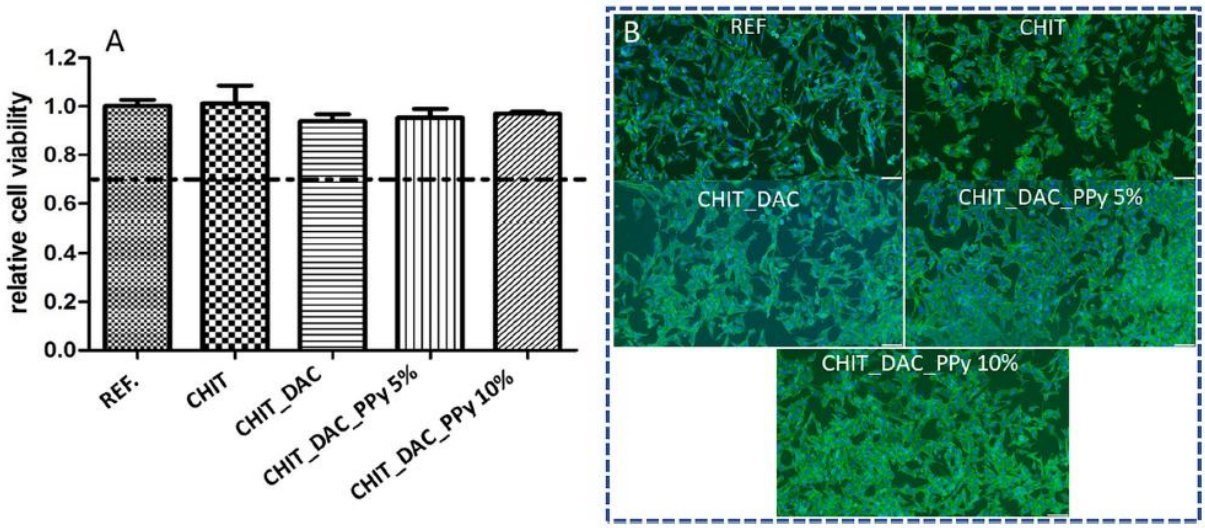

Fig. 6. A) Cytotoxicity of prepared chitosan hydrogel nanofibers; the dashed line represents the cytotoxicity threshold according to ISO 10993-5; B) cell growth on culture plastic in the presence of samples.

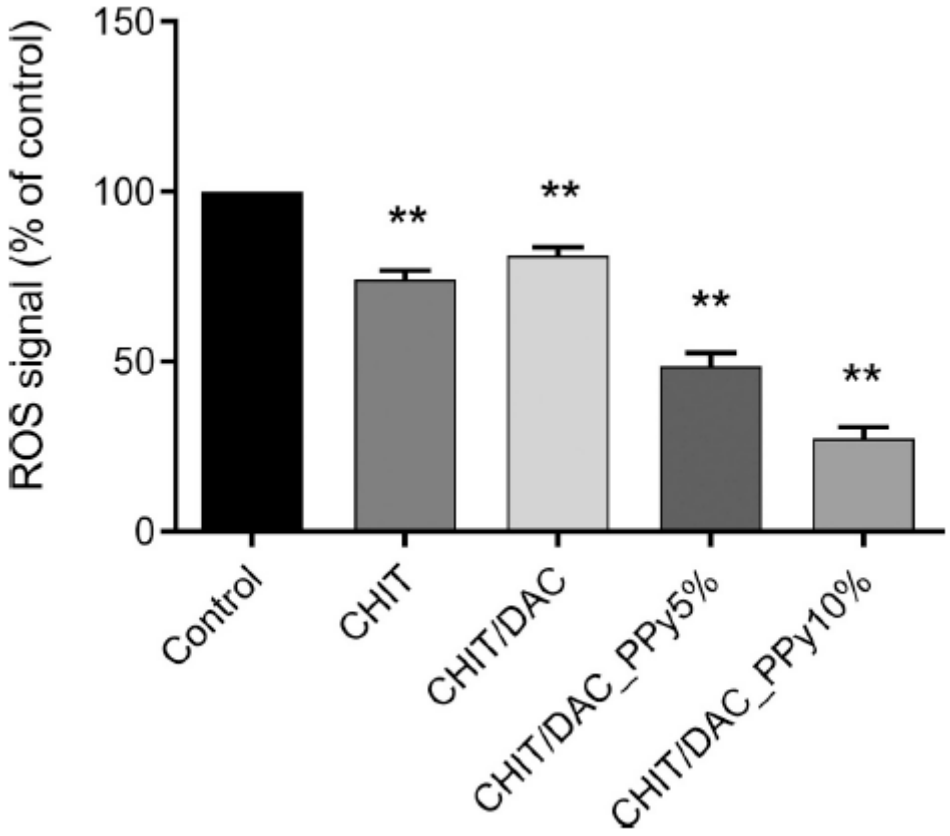

Fig. 7. The ROS signal reduction of prepared CHIT and their composites. The data were normalized to a percentage of the control group (without nanofibers) and presented as the mean $\pm SEM$ ($n = 4$), ($^{**}p < 0.01$).

The results (**Fig. 8**) show that $CHIT$ and $CHIT\_DAC$ samples only slightly decrease the spontaneous production of reactive oxygen species (ROS) to around 85 % compared to the control (not significant). In contrast, samples containing colloidal polypyrrole (PPy), show a significantly lower ROS signal at around 50-60 % compared to the control. Regarding ROS production of neutrophils activated by OZP and PMA, no significant decrease in ROS signal was observed for $CHIT$ and $CHIT\_DAC$. On the other hand, the antioxidant activity of composite nanofibers decreases ROS production by approx. 50-70 % of control, thus exhibiting similar trends as in spontaneous ROS production. This is once again scaling with the increased amount of PPy.

3.3.2. Macrophage response

Macrophages play a key role in the healing process of skin wounds. Two main phenotypes of macrophages are involved: $M1$, present in the initial inflammatory phase, responsible for amplification of the local inflammatory response to disinfect damaged tissue, and $M2$, active in the later stage of wound healing, and promoting tissue and vasculature growth [**55**]. Stimulation of macrophages, e.g., by lipopolysaccharides (LPS), induces the production of pro-inflammatory mediators, including cytokines, chemokines, and nitric oxide (NO). In the conducted experiments, the production of NO and IL-6, important signaling molecules of macrophages, was monitored (**Fig. 9**). MTT assay results did not show any cytotoxic effects of the tested nanofibers on macrophages (**Fig. 9**A). Regarding NO production (nitrite levels), no significant reduction was observed for $CHIT$ and $CHIT\_DAC$, while only

a minor, yet significant, reduction was observed for PPy composites (**Fig. 9**B). On the contrary, no significant impact on IL-6 production was detected for all tested samples (**Fig. 9**C).

3.3.3. In vitro wound healing

An in vitro scratch assay using $NIH/3T3$ cells was used to investigate the influence of the prepared materials on wound healing and cell migration [**45**]; see **Fig. 10**A and B). The remaining open wound area after 10 h of incubation was 71 $\pm$ 1 % for the reference material, 66 $\pm$ 4 % for $CHIT$, 69 $\pm$ 13 % for $CHIT\_DAC$ nanofibers, 58 $\pm$ 4 % for $CHIT\_-DAC\_PPy$ 5 %, and a reduced 41 $\pm$ 4 % for $CHIT\_DAC\_PPy$ 10 % (lower values indicate improved wound closure). Among all samples, only those incorporating colloidal polypyrrole (PPy) significantly enhanced cell migration and thus wound healing, with $CHIT\_DAC\_PPy$ 10 % showing the highest effect.

3.3.4. Antibacterial aktivity

The antibacterial activity of nanofibers was tested against $E.coli$ (Gram-negative) and $S.aureus$ (Gram-positive) bacteria according to the modified ISO 20743 and ISO 22196 standards, which cover the antimicrobial efficacy properties and test methods for plastic products, filters, nanofibers, or light and porous samples. These standards assess the ability of samples to inhibit (bacteriostatic) or kill (bactericidal) microorganisms over 24 h. The antimicrobial activity (A), i.e. the difference between the common logarithm of the arithmetic average of the number of bacteria obtained from functionalized samples after 24 h and 0 h of incubation, was determined using the equation outlined in Section S1.2. The evaluation of antibacterial effectiveness was conducted following EN ISO 20743:2021 Textiles - Determination of the antibacterial activity of textile products, with the corresponding effectiveness values presented in Table S3, where A $<$ 2 is low effectiveness, 2 $\leq$ A $<$ 3 is significant efficacy and A $\geq$ 3 is strong efficacy. Polyurethane nanofibers (PUR) without antibacterial activity were chosen as the reference. Photographs illustrating the dilution series of antimicrobial activity in the samples at 0 h and 24 h post-inoculation with $S.aureus$ and $E.coli$ are provided in SI (Figs. S1 and S2).

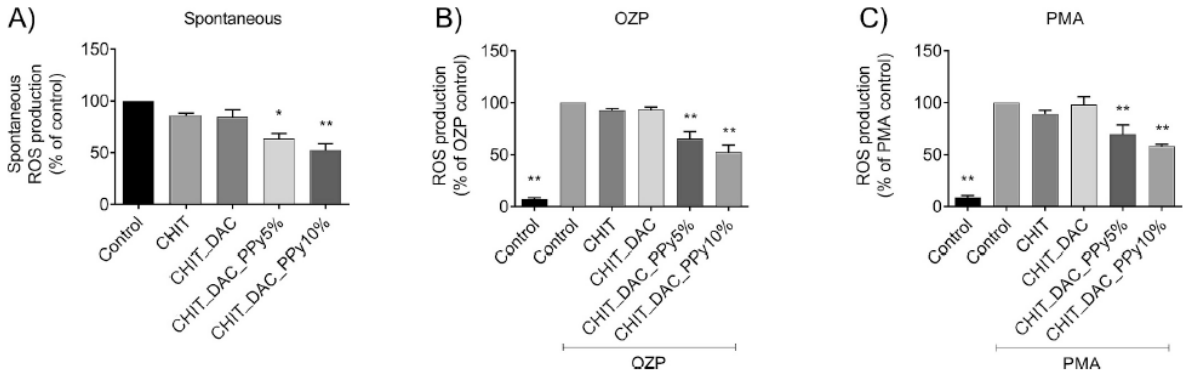

Fig. 8. A) The influence of $CHIT$ and their composites on the spontaneous production of ROS; B) ROS production activated by OZP in neutrophils; C) ROS production activated by PMA in neutrophils. The data were converted to percentage values relative to the corresponding control group (without nanofibers) and presented as mean ± standard error of the mean ($n = 4$), ($^{*}p < 0.05$, $^{**}p < 0.01$).

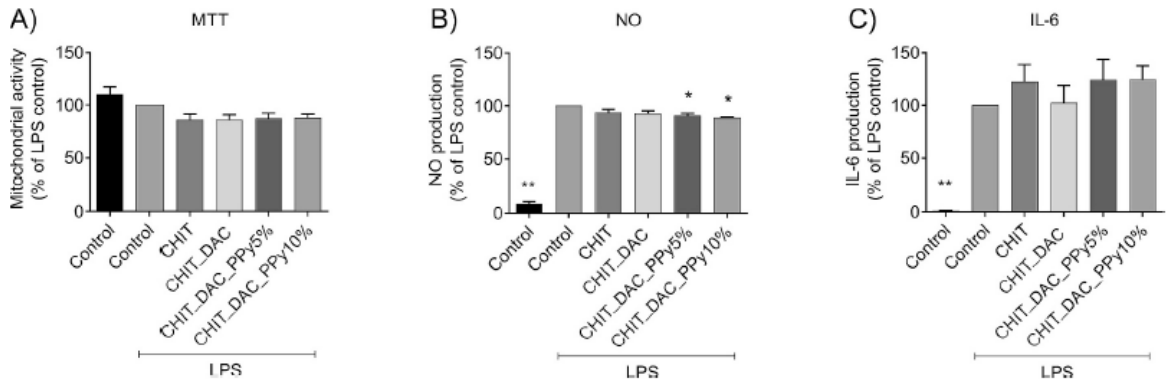

Fig. 9. The impact of $CHIT$ and their composites on the mitochondrial activity (A), NO production (B), and IL-6 production (C) in RAW264.7 macrophages following activation with 15 ng/mL LPS. Results were standardized to a percentage of the respective control and presented as mean $\pm SEM$ ($n = 4$). The data were converted to the percentage of the LPS control group (without nanofibers) and presented as mean $\pm$ standard error of the mean ($n = 4$), ($^{*}p < 0.05$, $^{**}p < 0.01$).

$CHIT$, $CHIT\_DAC$, $CHIT\_DAC\_PPy$ 5 %, and $CHIT\_DAC\_PPy$ 10 % samples showed antibacterial activity against the Gram-positive bacterium S. aureus CCM 4516 (**Table 2**). Specifically, $CHIT$ exhibited significant antibacterial activity (A = 2.598), while $CHIT\_DAC$ showed low antibacterial properties (A = 1.579). Free amine groups in chitosan are likely utilized during crosslinking with DAC, which consequently diminishes its antibacterial activity to some extent. The $CHIT\_DAC\_PPy$ 5 % and $CHIT\_DAC\_PPy$ 10 % composite nanofibers demonstrated significant antibacterial activity against gram-positive $S. aureus$, with A values of 6.783 and 6.746, respectively. The PPy in the composite thus syner-gistically interacts with chitosan, substantially enhancing its antibacterial efficacy against $S. aureus$.

Observed samples showed no antibacterial activity against $E. coli$ CCM 4517 (**Table 2**). This result contrasts with the general expectation that the positively charged chitosan groups would interact with the negatively charged surface of $E. coli$, inhibiting bacterial growth [**56**]. However, the antibacterial activity of chitosan is known to be variable, with some studies reporting a higher effect against $E. coli$, while others observe stronger inhibition of $S. aureus$ [**57**]. Other works report that the antibacterial action of chitosan depends on a series of factors related not only to the properties of chitosan itself [**58**] but also to the design of antibacterial tests, such as the time of exposure or the different origin of bacterial culture [**59**]. Among chitosan/polypyrrole composites, similar results were also observed for polypyrrole/soluble chitosan hydrogels, where significantly higher antibacterial action was observed against $S. aureus$ than against $E. coli$ [**19**].

While Gram-positive bacteria are more frequently associated with skin infections [**60**], the lower antibacterial activity against $E. coli$ observed in this study, which is primarily known as a pathogen in the intestines [**61**], highlights the complexity of interactions between the prepared materials and different bacterial strains. Given that some clinically significant Gram-negative pathogens, such as Pseudomonas aeruginosa, play an important role in wound infections [**62**], it would be beneficial to conduct further studies evaluating the material's broader antibacterial spectrum. Such research would help better understand its full potential and contribute to a more comprehensive evaluation of biomedical applications.

4. Conclusions

In this study, we have successfully prepared electrospun composite nanofibers based on crosslinked chitosan and PPy, whose properties overcome those of neat chitosan nanofibers prepared similarly. Chitosan was crosslinked by DAC during electrospinning, simplifying the whole process and providing a green alternative to current methods employing complex postprocessing steps and organic crosslinkers. DAC also tethers PPy particles, which were added as an active component to prepare composite nanofibers.

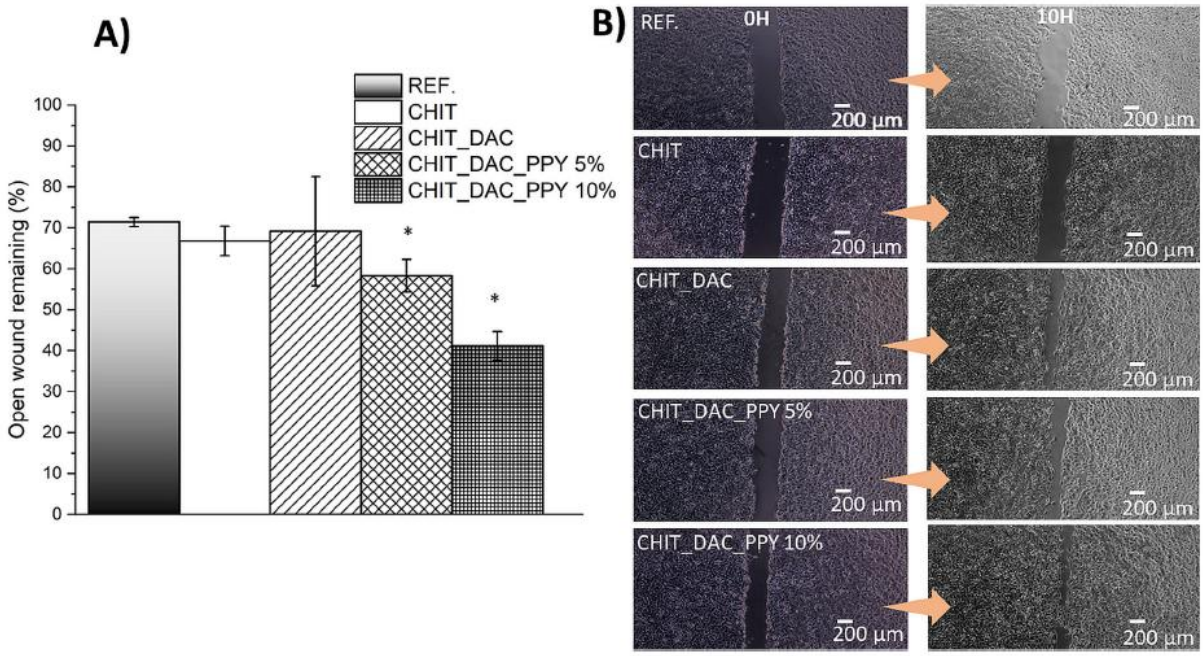

Fig. 10. Results of scratch assay on $NIH/3T3$ cell line. A) The remaining open area of the wound (%, lower is better) after 10 h of incubation in the presence of samples; B) representative figures of the wound after 0 h (left) and 10 h (right). ($^{*}p < 0.05$).

Table 2 Determination of the antibacterial activity (A) of prepared chitosan hydrogel nanofibers.

Sample	*Staphylococcus aureus* (A)	*Escherichia coli* (A)
CHIT	2.598	0.025
CHIT_DAC	1.579	0.028
CHIT_DAC_PPy 5 %	6.783	0.023
CHIT_DAC_PPy 10 %	6.746	0.152

All prepared samples were non-cytotoxic. Crosslinking by DAC increased the tensile strength of nanofibers and their stability at low pH compared to neat chitosan. The addition of PPy particles and formation of $CHIT\_DAC\_PPy$ composites significantly enhanced their ability to absorb fluids, improved antibacterial activity against gram-positive bacteria, greatly accelerated the wound healing in vitro, significantly increased antioxidant activity and reduced reactive oxygen species (ROS) production in both cell-free assay and in the presence of activated neutrophils, and slightly modulate the response of macrophages, all relative to neat chitosan nanofibers. However, no antibacterial activity was observed against $E.coli$, suggesting the need for further research to clarify the factors influencing the antibacterial activity of composite nanofibers.

Combined, the properties of fabricated composite nanofibers show their potential for possible wound dressings. However, further comprehensive biological testing, including in vivo tests, is essential to confirm their efficacy and safety before their application in biomedicine.

References

[1] J.D. Schiffman, C.L. Schauer, One-step electrospinning of cross-linked chitosan fibers, Biomacromolecules 8 (9) (2007) 2665-2667, **https://doi.org/10.1021/bm7006983**.

[2] R. Jayakumar, D. Menon, K. Manzoor, S.V. Nair, H. Tamura, Biomedical applications of chitin and chitosan based nanomaterials—a short review, Carbohydr. Polym. 82 (2) (2010) 227-232, **https://doi.org/10.10Wj. carbpol.2010.04.074**.

[3] R. Jayakumar, M. Prabaharan, S.V. Nair, H. Tamura, Novel chitin and chitosan nanofibers in biomedical applications, Biotechnol. Adv. 28 (1) (2010) 142-150, **https://doi.org/10.1016/j.biotechadv.2009.11.001**.

[4] S. Qasim, M. Zafar, S. Najeeb, Z. Khurshid, A. Shah, S. Husain, I. Rehman, Electrospinning of chitosan-based solutions for tissue engineering and regenerative medicine, Int. J. Mol. Sci. 19 (2) (2018) 407, **https://doi.org/10.3390/ ijms19020407**.

[5] R. Augustine, S.R.U. Rehman, R. Ahmed, A.A. Zahid, M. Sharifi, M. Falahati, A. Hasan, Electrospun chitosan membranes containing bioactive and therapeutic agents for enhanced wound healing, Int. J. Biol. Macromol. 156 (2020) 153-170, **https://doi.org/10.1016/j.ijbiomac.2020.03.207**.

[6] M. Pakravan, M.-C. Heuzey, A. Ajji, A fundamental study of chitosan/PEO electrospinning, Polymer 52 (21) (2011) 4813-4824, **https://doi.org/10.1016/). polymer.2011.08.034**.

[7] K. Kalantari, A.M. Afifi, H. Jahangirian, T.J. Webster, Biomedical applications of chitosan electrospun nanofibers as a green polymer - review, Carbohydr. Polym. 207 (2019) 588-600, **https://doi.org/10.10Wj.carbpol.2018.12.011**.

[8] V. Kumar, N. Sharma, P. Janghu, R. Pasrija, M. Umesh, P. Chakraborty, S. Sarojini, J. Thomas, Synthesis and characterization of chitosan nanofibers for wound healing and drug delivery application, Journal of Drug Delivery Science and Technology 87 (2023) 104858, **https://doi.org/10.10Wj.jddst.2023.104858**.

[9] M.A. Matica, F.L. Aachmann, A. T0ndervik, H. Sletta, V. Ostafe, Chitosan as a wound dressing starting material: antimicrobial properties and mode of action, Int. J. Mol. Sci. 20(23), Article 23 (2019), **https://doi.org/10.3390/ijms20235889**.

[10] P. Humpolíček, V. Kašpárková, J. Pacherník, J. Stejskal, P. Bober, Z. Capáková, K. A. Radaszkiewicz, I. Junkar, M. Lehocký, The biocompatibility of polyaniline and polypyrrole: a comparative study of their cytotoxicity, embryotoxicity and impurity profile, Mater. Sci. Eng. C 91 (2018) 303-310, **https://doi.org/10.1016/j. msec.2018.05.037**.

[11] T. Nezakati, A. Seifalian, A. Tan, A.M. Seifalian, Conductive polymers: opportunities and challenges in biomedical applications, Chem. Rev. 118 (14) (2018) 6766-6843, **https://doi.org/10.1021/acs.chemrev.6b00275**.

[12] K. Skopalová, K.A. Radaszkiewicz, V. Kašpárková, J. Stejskal, P. Bober, I. Junkar, M. Mozetic, Z. Capáková, M. Lehocký, M. Kašparová, J. Pacherník, P. Humpolíček, Modulation of differentiation of embryonic stem cells by polypyrrole: the impact on neurogenesis, Int. J. Mol. Sci. 22(2), Article 2 (2021), **https://doi.org/10.3390/ ijms22020501**.

[13] S. Kácerová, Z. Víchová, K. Valášková, J. Vícha, L. Münster, V. Kašpárková, O. Vašíček, P. Humpolíček, Biocompatibility of colloidal polypyrrole, Colloids Surf. B Biointerfaces 232 (2023) 113605, **https://doi.org/10.1016/j. colsurfb.2023.113605**.

[14] A.J.I. Petty, R.L. Keate, B. Jiang, G.A. Ameer, J. Rivnay, Conducting polymers for tissue regeneration in vivo, Chem. Mater. 32 (10) (2020) 4095-4115, **https://doi. org/10.1021/acs.chemmater.0c00767**.

[15] G. Shi, M. Rouabhia, Z. Wang, L.H. Dao, Z. Zhang, A novel electrically conductive and biodegradable composite made of polypyrrole nanoparticles and polylactide, Biomaterials 25 (13) (2004) 2477-2488, **https://doi.org/10.10Wj. biomaterials.2003.09.032**.

[16] M. Talikowska, X. Fu, G. Lisak, Application of conducting polymers to wound care and skin tissue engineering: a review, Biosens. Bioelectron. 135 (2019) 50-63, **https://doi.org/10.10Wj.bios.2019.04.001**.

[17] J. Zhang, C. Wu, Y. Xu, J. Chen, N. Ning, Z. Yang, Y. Guo, X. Hu, Y. Wang, Highly stretchable and conductive self-healing hydrogels for temperature and strain sensing and chronic wound treatment, ACS Appl. Mater. Interfaces 12 (37) (2020) 40990-40999, **https://doi.org/10.1021/acsami.0c08291**.

[18] B. Guo, P.X. Ma, Conducting polymers for tissue engineering, Biomacromolecules 19 (6) (2018) 1764-1782, **https://doi.org/10.1021/acs.biomac.8b00276**.

[19] S. Káčerová, M. Muchová, H. Doudová, L. Münster, B. Hanulíková, K. Valášková, V. Kašpárková, I. Kuřitka, P. Humpolíček, Z. Víchová, O. Vašíček, J. Vícha, Chitosan/dialdehyde cellulose hydrogels with covalently anchored polypyrrole: novel conductive, antibacterial, antioxidant, immunomodulatory, and antiinflammatory materials, Carbohydr. Polym. 327 (2024) 121640, **https://doi.org/ 10.1016/j.carbpol.2023.121640**.

[20] R. Cruz-Silva, E. Amaro, A. Escamilla, M.E. Nicho, S. Sepulveda-Guzman, L. Arizmendi, J. Romero-Garcia, F.F. Castillon-Barraza, M.H. Farias, Biocatalytic synthesis of polypyrrole powder, colloids, and films using horseradish peroxidase, J. Colloid Interface Sci. 328 (2) (2008) 263-269, **https://doi.org/10.10Wj. jcis.2008.09.021**.

[21] M. Zarei, A. Samimi, M. Khorram, M.M. Abdi, S.I. Golestaneh, Fabrication and characterization of conductive polypyrrole/chitosan/collagen electrospun nanofiber scaffold for tissue engineering application, Int. J. Biol. Macromol. 168 (2021) 175-186, **https://doi.org/10.1016/j.ijbiomac.2020.12.031**.

[22] A.M. Abdelgawad, S.M. Hudson, O.J. Rojas, Antimicrobial wound dressing nanofiber mats from multicomponent (chitosan/silver-NPs/polyvinyl alcohol) systems, Carbohydr. Polym. 100 (2014) 166-178, **https://doi.org/10.1016/j. carbpol.2012.12.043**.

[23] T. Furuike, T. Chaochai, T. Okubo, T. Mori, H. Tamura, Fabrication of nonwoven fabrics consisting of gelatin nanofibers cross-linked by glutaraldehyde or N-acetyl-d-glucosamine by aqueous method, Int. J. Biol. Macromol. 93 (2016) 1530-1538, **https://doi.org/10.1016/j.ijbiomac.2016.03.053**.

[24] M.R. Safaee-Ardakani, A. Hatamian-Zarmi, S.M. Sadat, Z.B. Mokhtari-Hosseini, B. Ebrahimi-Hosseinzadeh, J. Rashidiani, H. Kooshki, Electrospun Schizophyllan/ polyvinyl alcohol blend nanofibrous scaffold as potential wound healing, Int. J. Biol. Macromol. 127 (2019) 27-38, **https://doi.org/10.10Wj. ijbiomac.2018.12.256**.

[25] J.D. Schiffman, C.L. Schauer, Cross-linking chitosan nanofibers, Biomacromolecules 8 (2) (2007) 594-601, **https://doi.org/10.1021/bm060804s**.

[26] U.-J. Kim, Y.R. Lee, T.H. Kang, J.W. Choi, S. Kimura, M. Wada, Protein adsorption of dialdehyde cellulose-crosslinked chitosan with high amino group contents, Carbohydr. Polym. 163 (Supplement C) (2017) 34-42, **https://doi.org/10.1016/j. carbpol.2017.01.052**.

[27] M. Muchová, L. Münster, A. Vávrová, Z. Capáková, I. Kuřitka, J. Vícha, Comparison of dialdehyde polysaccharides as crosslinkers for hydrogels: the case of poly(vinyl alcohol), Carbohydr. Polym. 279 (2022) 119022, **https://doi.org/10.10Wj. carbpol.2021.119022**.

[28] D.P. Speer, M. Chvapil, C.D. Eskelson, J. Ulreich, Biological effects of residual glutaraldehyde in glutaraldehyde-tanned collagen biomaterials, J. Biomed. Mater. Res. 14 (6) (1980) 753-764, **https://doi.org/10.1002/jbm.820140607**.

[29] C. Cui, S. Sun, S. Wu, S. Chen, J. Ma, F. Zhou, Electrospun chitosan nanofibers for wound healing application, Engineered Regeneration 2 (2021) 82-90, **https://doi. org/10.1016/j.engreg.2021.08.001**.

[30] U.-J. Kim, S. Kuga, M. Wada, T. Okano, T. Kondo, Periodate oxidation of crystalline cellulose, Biomacromolecules 1 (3) (2000) 488-492, **https://doi.org/10.1021/ bm0000337**.

[31] M. Muchová, L. Münster, Z. Capáková, V. Mikulcová, I. Kuřitka, J. Vícha, Design of dialdehyde cellulose crosslinked poly(vinyl alcohol) hydrogels for transdermal drug delivery and wound dressings, Mater. Sci. Eng. C 116 (2020) 111242, **https:// doi.org/10.1016/j.msec.2020.111242**.

[32] L. Münster, Z. Capáková, M. Fišera, I. Kuřitka, J. Vícha, Biocompatible dialdehyde cellulose/poly(vinyl alcohol) hydrogels with tunable properties, Carbohydr. Polym. 218 (2019) 333-342, **https://doi.org/10.1016/j.carbpol.2019.04.091**.

[33] L. Münster, J. Vícha, J. Klofáč, M. Masař, A. Hurajová, I. Kuřitka, Dialdehyde cellulose crosslinked poly(vinyl alcohol) hydrogels: influence of catalyst and crosslinker shelf life, Carbohydr. Polym. 198 (2018) 181-190, **https://doi.org/ 10.1016/j.carbpol.2018.06.035**.

[34] K. Wegrzynowska-Drzymalska, P. Grebicka, D.T. Mlynarczyk, D. Chelminiak-Dudkiewicz, H. Kaczmarek, T. Goslinski, M. Ziegler-Borowska, Crosslinking of chitosan with dialdehyde chitosan as a new approach for biomedical applications, Materials 13 (15) (2020) 3413, **https://doi.org/10.3390/ma13153413**.

[35] A. Důbravová, M. Muchová, D. Škoda, L. Lovecká, L. Šimoníková, I. Kuřitka, J. Vícha, L. Münster, Highly efficient affinity anchoring of gold nanoparticles on chitosan nanofibers via dialdehyde cellulose for reusable catalytic devices, Carbohydr. Polym. 323 (2024) 121435, **https://doi.org/10.10Wj. carbpol.2023.121435**.

[36] L. Münster, M. Fojtů, Z. Capáková, T. Vaculovič, M. Tvrdočová, I. Kuřitka, M. Masařík, J. Vícha, Selectively oxidized cellulose with adjustable molecular weight for controlled release of

platinum anticancer drugs, Biomacromolecules 20 (4) (2019) 1623-1634, **https://doi.org/10.1021/acs.biomac.8b01807**.

[37] S. Mengistu Lemma, F. Bossard, M. Rinaudo, Preparation of pure and stable chitosan nanofibers by electrospinning in the presence of poly(ethylene oxide), Int. J. Mol. Sci. 17 (11) (2016) 1790, **https://doi.org/10.3390/ijms17111790**.

[38] P.J. Flory, J. Rehner, Statistical mechanics of cross-linked polymer networks II. Swelling, J. Chem. Phys. 11 (11) (1943) 521-526, **https://doi.org/10.1063/ 1.1723792**.

[39] M.R. Kasaai, Determination of the degree of N-acetylation for chitin and chitosan by various NMR spectroscopy techniques: a review, Carbohydr. Polym. 79 (4) (2010) 801-810, **https://doi.org/10.1016/j.carbpol.2009.10.051**.

[40] Y.N. Georgiev, M.H. Ognyanov, H. Kiyohara, T.G. Batsalova, B.M. Dzhambazov, M. Ciz, P.N. Denev, H. Yamada, B.S. Paulsen, O. Vasicek, A. Lojek, H. Barsett, D. Antonova, M.G. Kratchanova, Acidic polysaccharide complexes from purslane, silver linden and lavender stimulate Peyer's patch immune cells through innate and adaptive mechanisms, Int. J. Biol. Macromol. 105 (2017) 730-740, **https:// doi.org/10.1016/j.ijbiomac.2017.07.095**.

[41] O. Vasicek, A. Lojek, V. Jancinova, R. Nosal, M. Ciz, Role of histamine receptors in the effects of histamine on the production of reactive oxygen species by whole blood phagocytes, Life Sci. 100 (1) (2014) 67-72, **https://doi.org/10.1016/j. lfs.2014.01.082**.

[42] Z. Moosova, M. Pekarova, L.S. Sindlerova, O. Vasicek, L. Kubala, L. Blaha, O. Adamovsky, Immunomodulatory effects of cyanobacterial toxin cylindrospermopsin on innate immune cells, Chemosphere 226 (2019) 439-446, **https://doi.org/10.1016/j.chemosphere.2019.03.143**.

[43] E. Mosejová, R. Bosnjakovic, L. Kubala, O. Vasíček, Pseurotin D induces apoptosis through targeting redox sensitive pathways in human lymphoid leukemia cells, Antioxidants 10 (10) (2021) 1576, **https://doi.org/10.3390/antiox10101576**.

[44] O. Vasicek, D. Rubanova, B. Chytkova, L. Kubala, Natural pseurotins inhibit proliferation and inflammatory responses through the inactivation of STAT signaling pathways in macrophages, Food Chem. Toxicol. 141 (2020) 111348, **https://doi.org/10.1016Zj.fct.2020.111348**.

[45] C.-C. Liang, A.Y. Park, J.-L. Guan, In vitro scratch assay: a convenient and inexpensive method for analysis of cell migration in vitro, Nat. Protoc. 2 (2) (2007) 329-333, **https://doi.org/10.1038/nprot.2007.30**.

[46] L. Münster, J. Vícha, J. Klofáč, M. Masař, P. Kucharczyk, I. Kuřitka, Stability and aging of solubilized dialdehyde cellulose, Cellulose 24 (7) (2017) 2753-2766, **https://doi.org/10.1007/s10570-017-1314-x**.

[47] B. Weng, R. Shepherd, J. Chen, G.G. Wallace, Gemini surfactant doped polypyrrole nanodispersions: an inkjet printable formulation, J. Mater. Chem. 21 (6) (2011) 1918-1924, **https://doi.org/10.1039/C0JM02595J**.

[48] M. Fernandes Queiroz, K.R.T. Melo, D.A. Sabry, G.L. Sassaki, H.A.O. Rocha, Does the use of chitosan contribute to oxalate kidney stone formation? Mar. Drugs 13 (1) (2015) 1 **https://doi.org/10.3390/md13010141**.

[49] J.E. Dos Santos, E.R. Dockal, E.T.G. Cavalheiro, Synthesis and characterization of Schiff bases from chitosan and salicylaldehyde derivatives, Carbohydr. Polym. 60 (3) (2005) 277-282, **https://doi.org/10.1016/j.carbpol.2004.12.008**.

[50] R. Heras-Mozos, R. Hernández, R. Gavara, P. Hernández-Munoz, Dynamic covalent chemistry of imines for the development of stimuli-responsive chitosan films as carriers of sustainable antifungal volatiles, Food Hydrocoll. 125 (2022) 107326, **https://doi.org/10.1016/j.foodhyd.2021.107326**.

[51] F.A. Duck, Chapter 6—electrical properties of tissue, in: F.A. Duck (Ed.), Physical Properties of Tissues, Academic Press, 1990, pp. 167-223, **https://doi.org/10.1016/B978-0-12-222800-1.50010-3**.

[52] M. Bagheri, M. Validi, A. Gholipour, P. Makvandi, E. Sharifi, Chitosan nanofiber biocomposites for potential wound healing applications: antioxidant activity with synergic antibacterial effect, Bioengineering & Translational Medicine 7 (1) (2022) e10254, **https://doi.org/10.1002/btm2.10254**.

[53] M. Gizdavic-Nikolaidis, J. Travas-Sejdic, G.A. Bowmaker, R.P. Cooney, C.Thompson, P.A. Kilmartin, The antioxidant activity of conducting polymers in biomedical applications, Curr. Appl. Phys. 4 (2-4) (2004) 347-350, **https://doi. org/10.1016/j.cap.2003.11.045**.

[54] E. Nazarzadeh Zare, M. Mansour Lakouraj, M. Mohseni, Biodegradable polypyrrole/dextrin conductive nanocomposite: synthesis, characterization, antioxidant and antibacterial activity, Synth. Met. 187 (2014) 9-16, **https://doi. org/10.1016/j.synthmet.2013.09.045**.

[55] C. Chen, T. Liu, Y. Tang, G. Luo, G. Liang, W. He, Epigenetic regulation of macrophage polarization in wound healing, Burns & Trauma 11 (2023) tkac057, **https://doi.org/10.1093/burnst/tkac057**.

[56] E.I. Rabea, M.E.-T. Badawy, C.V. Stevens, G. Smagghe, W. Steurbaut, Chitosan as antimicrobial agent: applications and mode of action, Biomacromolecules 4 (6) (2003) 1457-1465, **https://doi.org/10.1021/bm034130m**.

[57] R.C. Goy, D. de Britto, O.B.G. Assis, A review of the antimicrobial activity of chitosan, Polímeros 19 (2009) 241-247, **https://doi.org/10.1590/S0104-14282009000300013**.

[58] C. Ardean, C.M. Davidescu, N.S. Nemes, A. Negrea, M. Ciopec, N. Duteanu, P. Negrea, D. Duda-Seiman, V. Musta, Factors influencing the antibacterial activity of chitosan and chitosan modified by functionalization, Int. J. Mol. Sci. 22 (14) (2021) 7449, **https://doi.org/10.3390/ijms22147449**.

[59] M.E. de F.A.G. de Oliveira, C.A. Peixoto, R.V. da S. Amorim, Ultrastructural analysis of chitosan antibacterial activity against clinical isolates of Staphylococcus aureus and Escherichia coli, Adv. Microbiol. 09 (10) (2019) 10, **https://doi.org/ 10.4236/aim.2019.910055**.

[60] C.P. Parlet, M.M. Brown, A.R. Horswill, Commensal staphylococci influence Staphylococcus aureus skin colonization and disease, Trends Microbiol. 27 (6) (2019) 497-507, **https://doi.org/10.1016/j.tim.2019.01.008**.

[61] M. Pasqua, V. Michelacci, M.L. Di Martino, R. Tozzoli, M. Grossi, B. Colonna, S. Morabito, G. Prosseda, The intriguing evolutionary journey of Enteroinvasive E. coli (EIEC) toward pathogenicity, Front. Microbiol. 8 (2017) 2390, **https://doi. org/10.3389/fmicb.2017.02390**.

[62] R. Serra, R. Grande, L. Butrico, A. Rossi, U.F. Settimio, B. Caroleo, B. Amato, L. Gallelli, S. De Franciscis, Chronic wound infections: the role of Pseudomonas aeruginosa and Staphylococcus aureus, Expert Rev. Anti Infect. Ther. 13 (5) (2015) 605-613, **https://doi.org/10.1586/14787210.2015.1023291**.